This is our manuscript prepared for submittion to Applied Physics Letters. The final version of the published article can be found using its DOI: 10.1063/5.0028363

Carrier Recombination and Diffusion in High-Purity Diamond after Electron Irradiation and Annealing

P. Grivickas[1*], P. Ščajev[2], N. Kazuchits[3], S. Lastovski[4], L. F. Voss[1], A. M. Conway[1], A. Mazanik[3], O. Korolik[3], V. Bikbajevas[2] and V. Grivickas[2]

[1] Lawrence Livermore National Laboratory, 7000 East Ave., Livermore, California 94551, USA
[2] Institute of Photonics and Nanotechnology, Vilnius University, Sauletekio Av. 3, Vilnius 10257, Lithuania
[3] Department of Physics, Belarusian State University, Nezalezhnastsi Av. 4, Minsk 220030, Belarus
[4] Scientific-Practical Materials Research Center at the National Academy of Sciences of Belarus, Minsk 220072, Belarus

Abstract

Carrier transport mechanisms are studied in high purity CVD diamond irradiated with 6 MeV electrons in the 10^{12} - 10^{16} cm^{-2} dose range and annealed at different temperatures up to 1450 C^o. Lifetimes and diffusion coefficients are extracted using two different pump-probe techniques based on the free-carrier-absorption and the transient grating principles and correlated with the corresponding defect evolution from spectroscopic measurements. The neutral monovacancy is revealed to be the main carrier recombination center in the just irradiated diamond providing bipolar carrier lifetimes of few nanoseconds at the highest irradiation dose. During annealing, single vacancies keep aggregating into the di-vacancies at $\leq$ 1000 C^o and the extended vacancy clusters at 1450 C^o with the slightly reduced carrier capture cross sections.

* Email of the corresponding author: grivickas1@llnl.gov

This is our manuscript prepared for submittion to Applied Physics Letters. The final version of the published article can be found using its DOI: 10.1063/5.0028363

Introduction

Design of semiconductor device structures requires control of carrier transport parameters which is commonly accomplished by using in-situ doping during the growth or thermal diffusion of implanted impurities. Electron irradiation is an alternative approach to optimize high frequency response in an accurate and cost-efficient way by introducing vacancies (V) and interstitials (I) [Hazdra 2004]. These point defects are produced during the inelastic collisions of electrons with the lattice and act as additional recombination centers with a certain capture cross-section. Assuming that the starting carrier lifetimes are long enough, the desired value is achieved by exposing a device to a well-calibrated dose of electrons at a certain energy. Both V and I, however, are relatively mobile at elevated temperatures leading to the intricate formation of secondary clusters and complexes with other impurities. In Si, for example, evolution of the divacancy related defects during the post-processing annealing is still an active research topic despite the decades' long history of investigations [Brotherton 1982, Krasko 2019].

In diamond, studies of electron irradiation created defects have their roots in high-energy physics were particle detectors are exposed to high irradiation doses (HID). It was found that direct annihilation of the V-I pairs in this material has very low probability at temperatures < 1900 C^o due to the large energy barrier of the process itself [Newton 2002] and the different activation energies for their mobility [Iakoubovskii 2003, Kiflawi 2007]. Under annealing, therefore, these defects migrate and form of a variety of secondary defects which depend the depth distribution of irradiation and on the sample impurity content. Large fraction of these defects shows up in the visible spectrum and has been utilized for color treatment of diamond specimens [Zaitsev 2017, 2018, Luhmann 2018]. In recent years, evolution of the nitrogen-vacancy (NV) center has attracted significant interest for applications ranging from biolabeling to quantum computing due to its quantum optical properties [Bourgeois 2020].

Despite the extensive research, effect of electron irradiation on carrier lifetimes and other transport parameters is virtually unknown in diamond. The underlying reason for this most likely is the absence of commercially viable electronic devices due to the complicated *n*-type doping. Diamond, however, has a tremendous potential in photoconductive (PC) switching applications where bulk device structures are predicted to take full advantage of high carrier mobility, high break-down electric field, and excellent thermal conductivity of this material [Hall 2020]. Such devices also capitalize on the advances in the chemical vapor deposition (CVD) growth of thick homoepitaxial crystals where levels of impurities can be reduced to several ppb levels. The highest carrier mobilities and lifetimes are usually reported in this high purity grade of diamond [Akimoto 2016, Scajev 2017]. Control of these transport parameters is, however, required to achieve optimized switching performance.

In this work, we investigate systematic transformation of carrier recombination and diffusion mechanisms using electron irradiation under well-defined experimental conditions. The high purity CVD samples are exposed to low irradiation doses (LID) varying over four orders of magnitude and incrementally annealed up to the technologically relevant temperature of 1450 C^o. During all processing steps, carrier dynamics is studied using two pump-robe techniques based on the free-carrier-absorption (FCA) and the transient grating (TG) principles. The results are correlated with the data from optical spectroscopy techniques such as photoluminescence (PL), cathodoluminescence (CL), optical transmission (OT), Raman scattering and cw-PC. Our findings suggest that carrier lifetimes can be tailored in a

predictable manner over many orders of magnitude while carrier mobilities remain mildly affected. Annealing reverses effects to some extend with the most significant deviations happening at the highest temperature of 1450 C^o. We show that all these changes are related to thermal diffusion and agglomeration of the V defects.

Experiments and results

The set of six CVD-grown samples with the dimensions of 2x2x0.5 mm was purchased from Element Six. All samples were assigned by the supplier to the electronic grade which is specified to contain < 5 ppb of nitrogen (N) and < 1 ppb of boron (B) [Element Six]. N content in the samples was measured by the secondary ion mass spectroscopy and showed N levels to be at or below the detection limit of $1 \cdot 10^{14}$ cm^{-3}. Negligible concentration of other impurities in the samples was also corroborated by the 77 K measurement of PL and CL showing lack of impurity related inter-center peaks as compared to the free exciton lines, the OT measurements showing absence of sub-band gap absorption, the cw-PC measurements showing no conductivity at any sub-gap excitation wavelengths, and the micro-Raman measurements showing lack of line broadening. Sample irradiation was carried at a linear electron accelerator using the electron flux of $(1\text{-}2.5)\times 10^{-12}$ cm^{-2}/s. The total dose Φ in each of the six samples was evenly distributed in the $2x10^{12}$ - 10^{16} cm^{-2} range. A Faraday cup was used for the dose calibration. To provide uniform distribution of the irradiation created defects along the 0.5 mm thickness of the samples, we chose the 6 MeV energy electrons which are shown to have the mean propagation path of 8 mm along the [100] crystallographic exes in diamond [Campbell 2000].

Post-irradiation annealing was performed for 1 h at each incremental temperature using the same procedure as described in Ref. [Grivickas 2020]. After each annealing step, samples were etched in a chromic acid solution for 30 s to remove graphitization and other possible contamination from sample surfaces. The four annealing temperatures used in the experiments were chosen for the following reasons: At 600 C^o, it is shown that the mobility of the carbon interstitial I_C is fully inhibited [Newton 2002, Iakoubovskii 2003, Kiflawi 2007]; At 900 C^o, the earlies signs of the V thermal diffusion are detected; At 1000 C^o, most of the features related to the single V defects disappear from the optical spectra [Davies 1992, Steeds 2014]; At 1450 C^o, complexes and aggregates related to the original irradiation defects are shown to have stable structures [Jones 2009, Maki 2009]. The final 1450 C^o temperature also has a technological importance as it is used in the Si foundries. All annealing was done in Ar atmosphere except at 1450 C^o which was done in a vacuum.

First, carrier lifetimes were investigated using the pump-probe technique based on the FCA principles which have been described in detail before [Scajev 2017]. The 10 ps duration pulses originating from the third 355 nm harmonic of a Nd:YLF laser were used for carrier excitation. The 50 mJ/cm^2 energy density of the pump pulse was sufficient to generate the average carrier concentration of $\Delta N_0 = 4 \cdot 10^{16}$ cm^{-3} across the sample according to the 0.2 cm/GW two-photon absorption (TPA) coefficient at this wavelength [Almeida 2017]. The 4 ns duration pulses originating from the first 1053 nm harmonic of a different Nd:YLF laser were used for carrier detection. Carrier decays were obtained by measuring differential transmission of the probe at different delays with respect to the pump. Synchronization and delay between the two pulses were controlled electronically allowing observations even of the slow carrier decays characteristic to the high purity diamond with μs-long carrier lifetimes.

This is our manuscript prepared for submittion to Applied Physics Letters. The final version of the published article can be found using its DOI: 10.1063/5.0028363

Carrier lifetimes extracted from the measured FCA decays are summarized in Fig. 1 for different irradiation doses and different annealing temperatures. Before annealing (red symbols), decrease in carrier lifetimes is apparent at $\Phi \sim 5\times10^{13}$ cm^{-2} and exceeds two orders of magnitude at $\Phi = 10^{16}$ cm^{-2}. Under annealing, lifetimes do not change much at 600 C^o but gradually recover at higher temperatures. It has been shown that the shape of the carrier lifetime dependency versus Φ in irradiated semiconductors can be described using the following expression [Krasko 2019, Linnros 1993, Bhoraskar 1991]:

$$1/\tau = 1/\tau_0 + \Phi^s K, \quad (1)$$

where τ_0 is the carrier lifetime in the not irradiated material, and K is the radiation damage coefficient. The power parameter s in Eq. (1) is usually ignored in literature as the recombination rate $1/\tau$ has been demonstrated to be directly proportional to irradiation at higher doses making $s = 1$. Data fits using Eq. (1) are shown in Fig. 1 by the solid lines while the corresponding parameters of these fits are presented in Table 1. Up to and including 1000 C^o, the $s = 1$ slope is indeed maintained and the extracted K is similar to the ones reported for bulk Si and Ge [Bhoraskar 1991, Yoon 2005]. At 1450 C^o, however, the slope changes to $s = 0.7$ suggesting significant transformation in the recombination mechanism.

Next, carrier dynamics was investigated using the TG technique based the spatial modulation of excited carriers [Scajev 2017]. The same laser and the third harmonic were used to excite carriers as in the case of FCA measurements. This time, though, the pump beam was split into two equal parts to produce interfering fringes on a sample surface. The main advantage of the technique is simultaneous extraction of the carrier recombination lifetime τ_R and the diffusion D coefficient from the measured TG decay time τ_G according to the relation:

$$1/\tau_G = 1/\tau_R + 4\pi^2 D/\Lambda^2, \quad (2)$$

where Λ is the spatial period of the modulated fringes. Generated TG decay is detected by transmitting the first harmonic of the same laser through the modulated region and measuring the first order diffraction efficiency (DE) which is related to τ_G according to:

$$DE\ t \propto \left(\frac{\pi n_{eh} d \Delta N_0}{\lambda} \right)^2 \exp\left(-\frac{2t}{\tau_G} \right), \quad (3)$$

where n_{eh} is the proportionality factor related to a single electron-hole pair, d is the effective absorption depth, λ is the excitation wavelength and ΔN_0 is the initial concentration of the excited carriers. Eq. (3) also allows to evaluate carrier generation mechanism by tracking DE values at $t = 0$ (DE_0) versus the excitation density. Such data are summarized in Fig. 2 (a) for the different Φ samples. Data are plotted on a log-log scale to reveal the p power slope of the DE_0 dependency. In the not irradiated sample (black), the dependence matches $p = 4$ (solid line) which originates from the square dependency implicit in the ΔN_0 term due to the TPA process and the another square in the preexponential term of Eq. (3) containing ΔN_0. In the irradiated samples, an additional DE_0 component emerges at lower excitations and increases

in amplitude with increasing Φ. The new component has the $p = 2$ dependency (solid lines) indicating a monopolar carrier generation in this excitation region.

Carrier lifetimes and diffusion coefficients were extracted at different excitations covering both $p = 4$ and $p = 2$ generation regions. At each excitation, the τ_G fit to the $DE(t)$ decay was repeated for several TG periods Λ and plotted in the $1/\tau_G$ versus $1/\Lambda^2$ fashion. The τ_R and D parameters in such plots correspond, respectively, to the intercept of the $1/\tau_G$ axes and the slope of the curve. Carrier lifetimes τ_R detected in the samples with the irradiation doses > 10^{14} cm^{-2} are shown in Fig. 2 (b). In the $p = 4$ region, the results are collected up to the 100 ns detection limit of the TG measurements and agree well with the earlier FCA results reproduced from Fig. 1. In the $p = 2$ region, the TG data reveal a drop in carrier lifetimes by almost two orders of magnitude. The eye guiding solid curves suggest an s-shape dependency which is preserved between samples with different irradiation. The shape is in stark contrast to the one in the not irradiated diamond as represented by the dashed gray area in Fig. 2 (b) encompassing the span of values reported in high quality CVD diamond [Scajev 2017, Grivickas 2020]. In the latter data, the longest lifetimes are observed at low excitations with the following decrease at large excitations attributed to the excitonic effects [Scajev 2017, Ichii 2020]. Carrier diffusion coefficients D obtained from the analysis of the same TG data sets are shown in Fig. 2 (c). The result is again compared to the data in the not irradiated diamond (gray curve) showing the gradual decrease of diffusion coefficients at large excitations due to the excitonic effects [Scajev 2017]. At excitations above 10 mJ/cm^2, the TG results follow the ambient trend, but at excitations bellow 10 mJ/cm^2, D is reduced significantly with values approaching zero at the highest irradiation doses as shown by the eye guiding curves.

Annealing effects in Fig. 3 are demonstrated using the $\Phi = 5 \cdot 10^{15}$ cm^{-2} sample as the example due to its largest 1.65 μs ambient lifetime among other samples. At temperatures up to and including 1000 C^o, the monopolar DE_0 amplitude was decreasing with increasing temperature as shown in Fig. 2 (d). Carrier lifetimes and diffusion, on the other hand, remained relatively unchanged as shown by the 1000 C^o data in Fig. 2 (e) and (f), respectively. At 1450 C^o, the decreasing trend of the monopolar DE_0 amplitude was reversed and, more importantly, it developed the $p = 1$ dependency as shown by the guiding dashed line. Carrier lifetimes at this temperature lost their *s*-shape dependency converging to the excitation independent values consistent with the data in Fig. 1. To confirm the finding, lifetimes were remeasured using the FCA technique in all irradiated samples and are summarized in Fig. 2 (e) by the solid symbols. Carrier diffusion, at the same time, showed slow reverse in the recovery towards ambient values though the changes were not very significant.

Discussion

The observed carrier transport changes were correlated with the defect evolution using primarily their signatures in the PL measurements at 77 K. In just irradiated samples, only the V related features were present. The most prominent peak at 741.15 nm was the zero-phonon line (ZPL) of the neutral state of the V^0 commonly referred to as the GR1 line [Davies 1992, Hunt 2000, Steeds 2014, Zaitsev 2017]. Emergence of this peak and its satellite at 744.6 nm is illustrated in Fig. 3 (a) for the $\Phi = 5 \cdot 10^{15}$ cm^{-2} sample which is chosen as an example throughout Fig. 3 due to its largest 1.65 μs ambient lifetime among other samples. The full

width half maximum (FWHM) of the GR1 peak at 0.8 ± 0.1 meV is sufficiently smaller than the 1.3 - 7.5 meV range reported for the IIa type diamond under HID range [Kiflawi 2007, Wang 2020] and indicates low degree of interaction between the point defects [Fisher 2006]. The inset of the Fig. 3 (a) shows that the V^0 defect is a good candidate to explain the linear lifetime decrease observed with the increasing Φ in Fig. 1. Traces of another V-peak were also detected at 393.5 nm (not shown) matching ZPL of the negative state V^- commonly referred to as the ND1 line [Twitchen 1999]. Two orders of magnitude smaller amplitude of this peak was consistent with the low N-donor concentration in our samples which is a main source to provide negative electron for the V^- formation.

Presence of V^0 can be quantified using OT measurements when converted into absorption units. At room temperature, ZPL of V^0 in the OT spectrum is overtaken by the phonon-assisted transitions forming the wide absorption band at ~ 2 eV as shown in Fig. 3 (b). The amplitude of the band increases linearly with Φ as shown by the inset and allows use the previously calibrated expression $N_{V0} = (\alpha_{2.0eV}/1.71)\times10^{17}$ cm^{-3} [Yelisseyev 2017] to extract V^0 concentration from the absorption cusp. The results extracted this way in our samples provide the production rate of vacancies $N_{V0}/\Phi = 2.4$ cm^{-1} which is close to the theoretical estimate of 2.85 cm^{-1} for 5 MeV electrons [Campbell 2000] and is higher of the experimental result of Hunt et al 2000 for 2 MeV. Assuming that V^0 acts as a single recombination center, its carrier capture cross section σ can be now estimated from $1/\tau = v\sigma N_{V0}$ expression, where $v = 2\cdot10^7$ cm^{-2} is the thermal carrier velocity in diamond. Using τ = 6.8 ns value at $\Phi = 5\cdot10^{15}$ cm^{-2} from Fig. 1, we obtain $\sigma_V = 6.3\cdot10^{-16}$ cm^{-2} which is larger than the one of $\sigma_N = 1\cdot10^{-16}$ cm^{-2} reported for N^0 center [Scajev 2017]. This indicates that V^0 is a quite effective lifetime killer.

Under annealing, the V^0 peak continues to dominate in the PL spectrum up to 1000 C^o as shown in Fig. 3 (a). At 600 C^o, the carbon di-interstitial line TR12 at 470.1 nm [Hunt 2000, Zaitsev 2017, Iakoubovskii 2003] has been also detected (not shown) but disappeared at 900 C^o. This suggests that I_C related defects do not contribute significantly to recombination process as τ remains relatively unaffected by their transformations. At 1000 C^o, the V^0 peak loses its strength considerably and becomes accompanied by the ZPL of divacancy V_2 line at 733.1 nm and its phonon satellite at 738 nm [Streeds 2014]. The V_2 line shows no stress-related splitting in contrast to the reported HID results [Streeds 2014] indicating again a high degree of crystallinity in our samples. In addition, the ZPL of NV^0 center at 575 nm (not shown) has shown considerable presence. Finally, at the highest temperature of 1450 C^o both V^0 and V_2 lines disappear and are replaced by a doublet at 736.6/736.9 nm identified as the SiV complex [Zaitsev 2017, Streeds 2014].

To better visualize correlation between the observed PL peaks and carrier recombination, Fig. 3 (c) shows the recombination rate 1/τ taken from the data in Fig. 1, and continuous progression of the normalized PL amplitudes in Fig. 3 (d) at the same temperatures. In the 900 C^o to 1000 C^o range, the V_2 cluster clearly takes over the recombination process as the significant loss of V^0 in this range is not reflected by the equivalent 1/τ drop. The assumption is also supported by the relative strength of the V_2 peak as compared to other candidates. At 1450 C^o, it appears that SiV and to less degree NV^0 become centers compensating for the V_2 loss as 1/τ remains relatively unchanged as compared to 1000 C^o. This assumption, however, contradicted by their Φ-dependence as shown in Fig. 3 (e). Dominant recombination center would be expected to have a linear amplitude increase like the one of the V_2 trace emerging at high Φ. The SiV shape, in

contrast, looks saturated after it emerges at moderate Φ. The NV^0 also shows the shape which correlates with the ambient lifetimes in each sample suggesting different content of N in them. The result is also supported by the similar dependence of the ZPL at 389 nm of N-related clusters of nitrogen atom and carbon interstitial – (NC) [Zaitsev 2017] detected in the CL spectra at 77 K.

We propose, therefore, that the new recombination center is closely related to the formation of the V multi-clusters. These defects are not detectable by the PL measurements but produce the "brown" coloration of both natural and CVD IIa diamonds by a featureless absorption spectrum above 1.5 eV [Jones 2009]. Such spectrum can be understood as gradually ramp transitions arising from filled low density states at the Fermi level to empty defect gap sates as proposed by Jones 2009. Fig. 3 (b) shows that exactly this type of spectrum develops in the electron irradiated sample at 1450 C in contrast to the 600 C and 1000 C spectra which are the smaller amplitude replicas of the just irradiated sample. Note, that absorption coefficient is weak and in according sorting classification by Fisher [2006], only the lowest brown color of 1^{st}-grade is achieved here for LID region. While the exact configuration of the multivacancy defects (lines or discs or other possible shapes) are still under debate, presence of these defects was clearly revealed by the positron annihilation spectroscopy [Maki 2009, Maki 2011].

The revealed V evolution also explains some features related to carrier transport. The inset of Fig. 3 (b) shows that the DE_0 amplitude associated with the monopolar generation in as irradiated samples has linear dependency on Φ at the excitation energy of 3.5 eV. This strongly suggests that the monopolar generation observed the TG measurements originates to the neutral state V^0. In general, V is an amphoteric defect with both 0/+ and 0/- charge transitions being possible within the bandgap [Deak 2014]. The 0/+ level lays ~ 1 eV above the valance band and remains inaccessible in our experiments as it requires > 4.2 eV photons to elevate an electron from the defect into the conduction band. The 0/- level, on the other hand, lays ~ 2 eV above the valance band and is easily reachable by the 3.5 eV photons leaving a free hole in the valence band after an electron is elevated into the defect. It is likely, that the holes generated this way stay in the vicinity of the charged defect due to the Coulomb attraction. This would explain both the observed drop in the carrier lifetimes because of the enhanced recombination probability and the observed drop in the carrier diffusivity because of the internal electric field. Under the bipolar generation, free carriers can recombine using transitions into both 0/+ and 0/- levels making V^0 an amphoteric recombination center. Such recombination process requires charge conservation and would account for the longer lifetimes depending on the specific capture cross sections [Klein ?]. It is not clear, however, why the energy inflection points of the s-shapes in Fig. 2 (b) do not have the one to one correlation with the irradiation dose.

Under annealing at ≤ 1000 C^o, the decrease of the monopolar DE_0 amplitude shown in the inset of Fig. 2 (d) resembles the annihilation of the V^0 defect shown in Fig. 3 (d) but is much smaller in the relative size due to the formation of the V_2 clusters. Turns out that the di-vacancy V_2 is also an amphoteric defect with both 0/+ and 0/- charge transitions levels being very close to the ones for the mono-vacancy [Deak 2014]. This explains small changes in carrier transport observed in this temperature range despite the transformation of defects. The V multi-clusters emerging at 1450 C^o, however, behave in a radically different behavior. The sub-linear $p = 1$ generation shown in Fig. 2 (d) implies that the absorption cross-section of the defect is no longer a constant but dependents on its overall charge. Similarly, the $s = 0.7$ slope detected for the Φ dependence in Fig. 1 stipulates the same for the carrier capture cross-

section. Another less likely alternative is that the size of V-clusters is increasing with increasing irradiation dose. Nevertheless, the cluster remains an active recombination center and, more importantly, does not transform into a simple charge trap at low excitations. These properties make V-cluster well suited for tuning response of photoconductive devices over a large operation range. To test the hypothesis, PC measurements were done in all samples using the same structure of the lateral contacts biased under constant illumination at 220 nm. Open symbols in Fig. 1 confirm that PC response follows the same trend as the carrier lifetimes measured using the FCA technique with 3.53 eV laser pulses.

Summary

In conclusion, we have measured carrier recombination and diffusion in high purity CVD diamond irradiated with 6 MeV electrons in the LID dose range below $1x10^{16}$ cm^{-2}. The radiation damage coefficient of K = 3e-8 cm^2/s is detected for the bipolar lifetime of free carriers generated through the TPA process. The result indicates that the 1 GHz response can be achieved in diamond devices with electron doses < $1x10^{17}$ cm^{-2}. The neutral monovacancy is revealed to be the most likely center responsible for the recombination process. Under annealing, the V-defect diffuses and aggregates forming clusters at 1450 C^o. Charge transfer from and into these secondary defects is complicated as shown by the nonlinear bipolar lifetime dependence on the irradiation dose. The measured PC response, however, agrees well with these lifetimes providing control of carrier transport in diamond PC devices.

Acknowledgements

The authors are grateful to M. Rusetsky for CL spectra measurements and V. Kazuchits for cw-PC spectra measurements.

References

[Hazdra 2004] P. Hazdra, J. Vobecky, H. Dorschner, K. Brand, "Axial lifetime control in silicon power diodes by irradiation with protons, alphas, low- and high-energy electrons" Microelectronics Journal **35**, 249 (2004).

[Brotherton 1982] S. D. Brotherton, and P. Bradley, "Defect production and lifetime control in electron and γ-irradiated silicon" Journal of Applied Physics **53**, 5720 (1982);

[Krasko 2019] M. Krasko, A. Kolosiuk, V. Voitovych, and V. Povarchuk, "Lifetime Control in Irradiated and Annealed Cz n-Si: Role of Divacancy-Oxygen Defects" Phys. Status Solidi A**, 216**, 1900290 (2019);

[Newton 2002] M.E. Newton, B.A. Campbell, D. J. Twitchen, J.M. Baker, T.R. Anthony, "Recombination-enhanced diffusion of self-interstitial atoms and vacancy-interstitial recombination in diamond" Diamond and related materials **11**, 618 (2002).

[Iakoubovskii 2003] K. Iakoubovskii, I. Kiflawi, K. Johnston, A. Collins, G. Davies, A. Stesmans, "Annealing of vacancies and interstitials in diamond" Phys. B, **340-342**, 67 (2003).

[Kiflawi 2007] I. Kiflawi, A.T. Collins, Iakoubovskii, D. Fisher, "Electron irradiation and the formation of vacancy-interstitial pairs in diamond" J. Phys. Condens. Matter. **19**, 046216 (2007).

[Zaitsev 2017] A. M. Zaitsev, K. S. Moe, W. Wang, "Optical centers and their depth distribution in electron irradiated CVD diamond" DRM, **71**, 38 (2017).

[Zaitsev 2018] A. M. Zaitsev, K. S. Moe, W. Wang, "Defect transformations in nitrogen-doped CVD diamond during irradiation and annealing" DRM, **88**, 237 (2018).

[Luhmann 2018] T. Luhmann, N. Raatz, R. John, M. Lesik, J. Rodiger, M. Portail, D. Wildanger, F. Kleibler, K. Nordlund, A. Zaitsev, J-F. Roch, A. Tallaire, J. meijer, S. Pezzagna, "Screening and engineering of colour centres in diamond" J. Phys. D: Appl. Phys. **51**, 483002 (2018).

[Bourgeois 2020] E. Bourgeois, M. Gulka, M. Nesladek "Photoelectric detection and quantum readout of nitrogen-vacancy center spin states in diamond" Adv. Optical Mater. 1902132 (2020) DOI: 10.1002/adom.201902132.

[Hall 2020] D.L. Hall, L.F. Voss, P. Grivickas, M. Bora, A.M. Conway, P. Ščajev, V. Grivickas, "Photoconductive Switch With High Sub-Bandgap Responsivity in Nitrogen-Doped Diamond" IEEE El. Dev. Lett. **41**, 1070 (2020).

[Scajev 2017] P. Ščajev, „Excitation and temperature dependent exciton-carrier transport in CVD diamond: Diffusion coefficient, recombination liftime and diffusion length" Physica B **510**, 92 (2017).

[Akimoto 2016] I. Akimoto, N. Naka, N. Tokuda, Time-resolved cyclotron resonance on dislocation-free HPHT diamond, DRM **63**, 38 (2016).

[Element Six] S. Mathias, Element Six Technologies, 3rd Adamas Collaboration Meeting 19 November 2014, see http://www-adamas.gsi.de/ADAMAS03/talks/Mathias_E6.pdf.

[Campbell 2000] B. Campbell and A. Mainwood, „Radiation damage of diamond by electron and gamma irradiation" Phys. Stat. Sol. (a) **181**, 99 (2000).

[Grivickas 2020] P. Grivickas, P. Ščajev, N. Kazuchits, A. Mazanik, O. Korolik, L. F. Voss, A. M. Conway, D. L. Hall, M. Bora, L. Subačius, V. Bikbajevas, V. Grivickas, "Carrier recombination parameters in diamond after surface boron implantation and annealing" J. Appl. Phys. **127**, 245707 (2020).

[Davies 1992] G. Davies, S.C. Lawson, A.T. Collins, A. Mainwood, S. J. Sharp, " Vacancy related centers in diamond" Phys. Rev. B **46**, 13157 (1992).

[Steeds 2014] J.W. Steeds, and S. Kohn, "Annealing of electron radiation damage in a wide range of band IIa diamond samples", DRM, **50** 110 (2014).

[Jones 2009] R. Jones, "Dislocations, vacancies and the brown colour of CVD and natural diamond" DRM, **18**, 820 (2009).

[Maki 2009] J-M. Maki, F. Tuomisto, C.J. Kelly, D. Fisher, P.M. Martineau, "Properties of optically active vacancy clusters in type IIa diamond" J. Phys. Condens. Matter. **21**, 364216 (2009).

[Linnros 1993] J. Linnros, P. Norlin, A. Hallen, "A new technique for depth resolved carrier recombination measurements applied to proton irradiated thyristors" IEEE Tr. El. Dev. **40**, 2065 (1993).

[Bhoraskar 1991] V.N. Bhoraskar, S.D. Dhole, S. Singh, S.M. Jahagirdar, K.S. Srinivas, "Radiation damage and minority carrier lifetime in crystalline silicon" Nucl. Instr. & Meth. in Phys. Res. B **62**, 99 (1991).

[Yoon 2005] H. Yoon, K.M. Edmondson, G.S. Kinsey, R.R. King, P. Herbert, R.K. Ahrenkiel, B.T. Cavicchi, N.H. Karam, "Minority carrier lifetime and radiation damage coefficients of germanium" In Conference Record of the IEEE Photovoltaic Specialists Conference. p. 842-845 (2005).

[Ichii 2020] T. Ichii, Y. Hazama, N. Naka, K. Tanaka, "Study of detailed balance between excitons and free carriers in diamond using broadband terahertz time-domain spectroscopy" Appl. Phys. Lett. **116**, 231102 (2020).

[Hunt 2000] D.C. Hunt, D.J. Twitchen, M.E. Newton, J.M. Baker, T.R. Anthony, W.F. Banholzer, S.S. Vagarali, "Identification of the neutral carbon <100>-split interstitial in diamond" Phys. Rev. B **61**, 3863 (2000).

[Fisher 2006] D. Fisher, D.J.F. Evans, C. Glover, C.J. Kelly, M.J. Sheehy, G.C. Summerton, "The vacancy as a probe of the strain in type IIa diamonds" DRM **15**, 1636 (2006).

[Wang 2020] K. Wang, R. Guo, S. Ding, H. Wang, Y. Tian, Y. Wang, "Temperature dependence of optical centers in ultrapure diamond after 200 keV electron irradiation" J. Phys. D.: Appl. Phys. 122802R1 (2020).

[Yelisseyev 2017] A. Yelisseyev, V. Vins, V. Afanasiev, A. Rybak, "Effect of ekectron irradiation on optical absorption of impact diamonds from the Popigai meteorite crater" DRM **79**, 7 (2017).

[Maki 2011] J.-M. Maki, F. Tuomisto, A. Varpula, D. Fisher, R.U.A. Khan, P.M. Martineau, "Time-depemndence of charge transfer processes in diamond studied with positrons" Phys. Rev. Lett. **107**, 217403 (2011).

[Twitchen 1999] D. J. Twitchen, D. C. Hunt, V. Smart, M. E. Newton, J. M. Baker, "Correlation between ND1 optical absorption and the concentration of negative vacancies determined by electron paramagnetic resonance (EPR)" DRM, **8**, 1572 (1999).

[Deak 2014] P. Deak, B. Aradi, M. Kaviani, T. Frauenheim, A. Gali, "The formation of NV centers in diamond: A theoretical study based on calculated transitions and migration of nitrogen and vacancy related defects" Phys. Rev. B, **89**, 075203 (2014).

This is our manuscript prepared for submittion to Applied Physics Letters. The final version of the published article can be found using its DOI: 10.1063/5.0028363

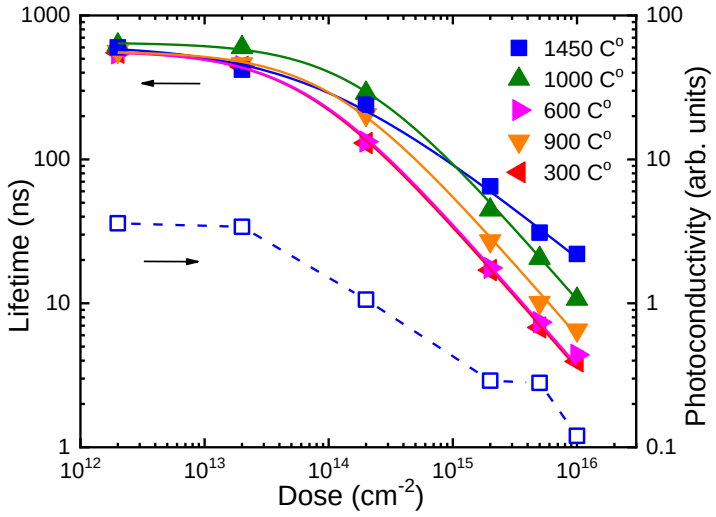

Fig. 1. Carrier lifetimes (solid symbols) in high purity diamond at different irradiation doses and annealing temperatures. Solid lines show data fits according Eq. (1). Open symbols show cw-PC in the samples annealed at 1450 C°.

TABLE 1. Fitting parameters for data in Fig. 1 using Eq. (1).

Treatment	τ_0 (ns)	K[×1e-8 cm^2/s]	s
Irrad 600 C	571 ± 5	2.8 ± 0.1	1 ± 0.03
	566 ± 7	2.7 ± 0.1	1 ± 0.03
900 C	564 ± 9	1.7 ± 0.1	1 ± 0.03
1000 C	648 ± 12	0.9 ± 0.1	1 ± 0.03
1450 C	626 ± 27	(3 ± 0.4)e4	0.7 ± 0.03

This is our manuscript prepared for submittion to Applied Physics Letters. The final version of the published article can be found using its DOI: 10.1063/5.0028363

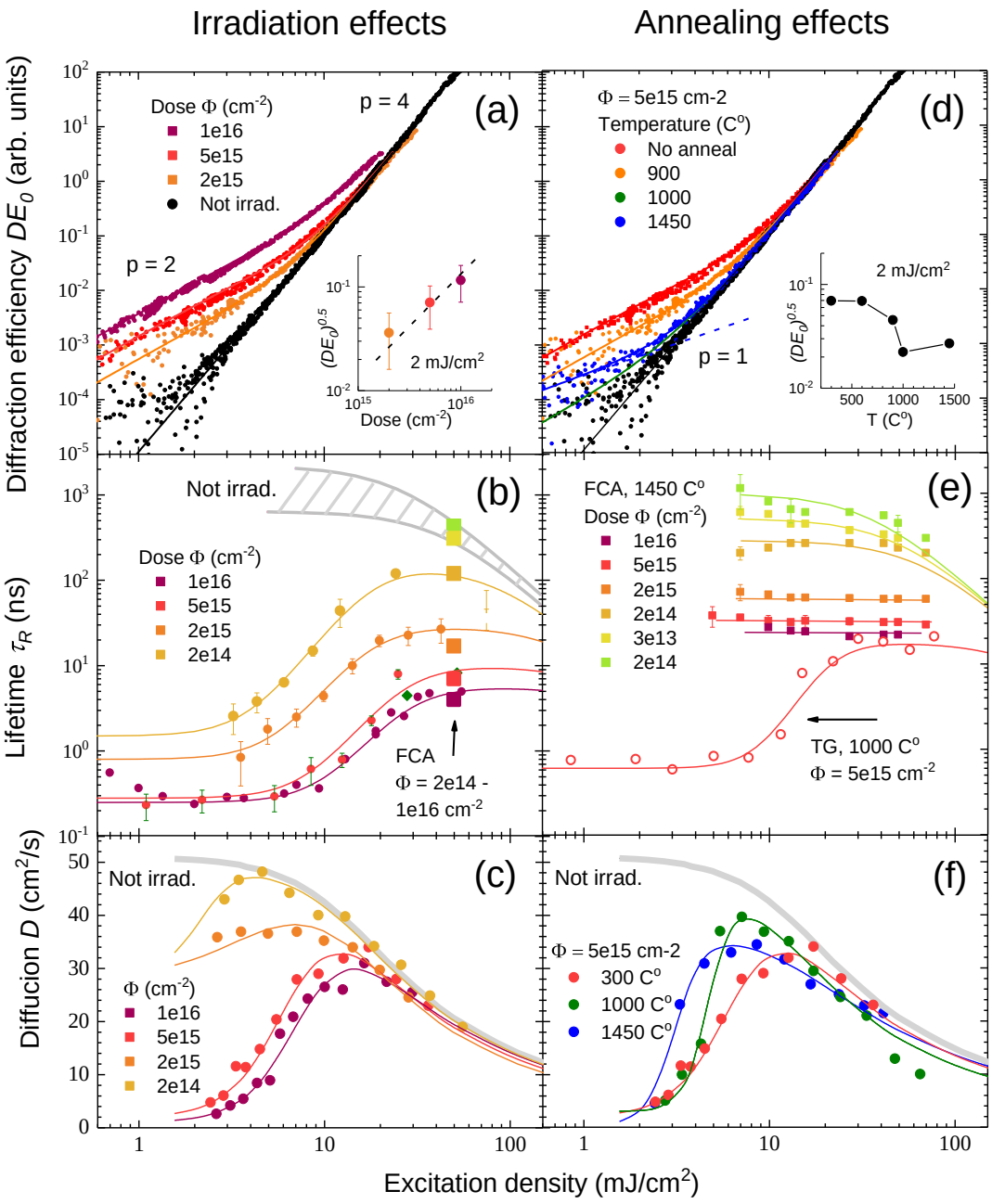

Fig. 2. Dependences of the diffraction efficiency (a, d), the carrier lifetime (b, e) and the diffusion coefficient (c, f) on the excitation density to elucidate irradiation effects (figures on the left) and annealing effects (figures on the right). In (a), p = 4 and p = 2 show power

This is our manuscript prepared for submittion to Applied Physics Letters. The final version of the published article can be found using its DOI: 10.1063/5.0028363

dependence corresponding to the TPA region and the monopolar generation region, respectively. In (d), p = 1 shows sub-linear power dependence after annealing at 1450 C^{o}. Insets in (a) and (d) show dependence of the monopolar amplitude on the dose and the temperature, respectively. In (b) and (e), the circles correspond to the TG data and the squares correspond to the FCA data. The gray region in (b) and the gray curves in (c) and (f) show ambient results in not irradiated diamond.

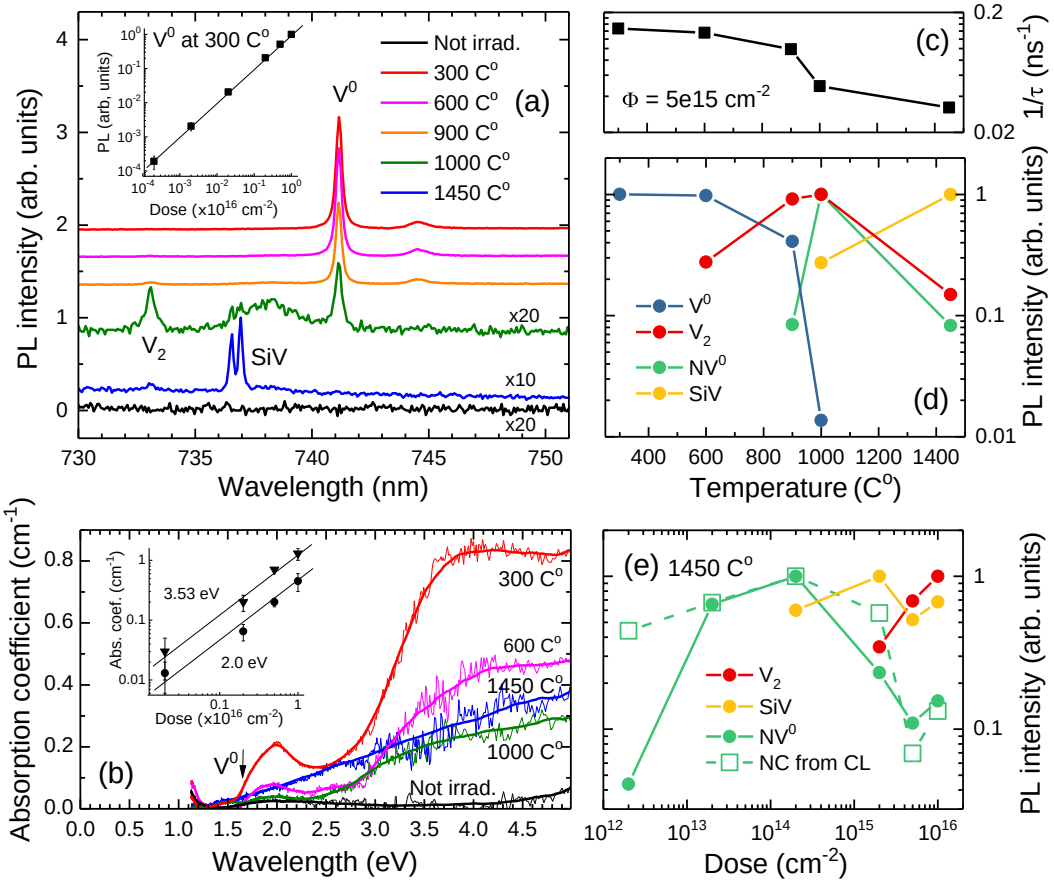

Fig. 3. (a) The 77 K PL spectra in diamond using 473 nm excitation before irradiation, after the Φ = 5·10^{15} e/cm^{-2} irradiation and at different annealing temperatures. Spectra are shifted on the vertical scale for better visibility. The inset shows the dependence of the V^0 line on the irradiation dose before annealing. (b) Absorption spectra at RT in the Φ = 5·10^{15} e/cm^{-2} irradiated sample at different annealing temperatures. The inset shows the dependence of the absorption coefficient at 2.0 eV and 3.53 eV versus the irradiation dose before annealing. (c) Recombination rate in the Φ = 5·10^{15} e/cm^{-2} irradiated sample versus annealing temperature. (d) Normalized PL intensities of different PL peaks versus the annealing temperature. (e) Normalized PL (solid symbols) and CL (open symbols) intensity versus the irradiation dose after annealing at 1450 C^{o}.

This is our manuscript prepared for submittion to Applied Physics Letters. The final version of the published article can be found using its DOI: 10.1063/5.0028363